

1 **Late Holocene Relative Sea-Level Reconstruction near Palmer Station, northern Antarctic Peninsula**  
2 **strongly controlled by Late Holocene ice mass changes**

3 Alexander R. Simms<sup>1</sup>, Pippa L. Whitehouse<sup>2</sup>, Lauren M. Simkins<sup>3</sup>, Grace Nield<sup>2</sup>, Regina DeWitt<sup>4</sup>, and  
4 Michael J. Bentley<sup>2</sup>

5 <sup>1</sup>Department of Earth Science, University of California Santa Barbara, 1006 Webb Hall, Santa Barbara,  
6 California 93106, U.S.A., [asimms@geol.ucsb.edu](mailto:asimms@geol.ucsb.edu), +1 805-893-7292

7 <sup>2</sup>Department of Geography, Durham University, DH1 3LE, United Kingdom,  
8 [pippa.whitehouse@durham.ac.uk](mailto:pippa.whitehouse@durham.ac.uk)

9 <sup>3</sup>Department of Environmental Sciences, University of Virginia, Clark Hall 205, 291 McCormick Road,  
10 Charlottesville, VA 22904, U.S.A., [lsimkins@virginia.edu](mailto:lsimkins@virginia.edu)

11 <sup>4</sup>Department of Physics, East Carolina University, Howell Science Complex, Rm C-209, 1000 E. 5<sup>th</sup> Street,  
12 Greenville, NC 27858, U.S.A., [dewittr@ecu.edu](mailto:dewittr@ecu.edu)

13  
14 **Abstract**

15 Many studies of Holocene relative sea-level (RSL) changes across Antarctica assume that their  
16 reconstructions record uplift from glacial isostatic adjustment caused by the demise of the Last Glacial  
17 Maximum (LGM) ice sheets. However, recent analysis of GPS observations suggests that mantle  
18 viscosity beneath the Antarctic Peninsula is weaker than previously thought, which would imply that  
19 solid Earth motion is not controlled by post-LGM ice-sheet retreat but instead by late Holocene ice-mass  
20 changes. If this hypothesis is correct, one might expect to find Holocene RSL records that do not reflect  
21 a monotonic decrease in the rate of RSL fall but show variations in the rate of RSL change through the  
22 Holocene. We present a new record of late Holocene RSL change from Torgersen Island near Palmer

23 Station in the western Antarctic Peninsula that shows an increase in the rate of relative sea-level fall  
24 from  $3.0 \pm 1.2$  mm/yr to  $5.1 \pm 1.8$  mm/yr during the late Holocene. Independent studies of the glacial  
25 history of the region provide evidence of ice-sheet changes over similar time scales that may be driving  
26 this change. When our RSL records are corrected for sea-surface height changes associated with glacial  
27 isostatic adjustment (GIA), the rate of post-0.79 ka land uplift at Torgersen Island,  $5.3 \pm 1.8$  mm/yr, is  
28 much higher than the rate of uplift recorded at a nearby GPS site at Palmer Station prior to the Larsen B  
29 breakup in 2002 AD (1998-2002 AD;  $<0.1$  mm/yr), but similar to the rates observed after 2002 AD (2002-  
30 2013 AD; 6-9 mm/yr). This substantial variation in uplift rates further supports the hypothesis that  
31 Holocene RSL rates of change are recording responses to late Holocene and recent changes in local ice  
32 loading rather than a post-LGM signal across portions of the Antarctic Peninsula. Thus Middle-to-Late  
33 Holocene RSL data may not be an effective tool for constraining the size of the LGM ice sheet across  
34 portions of the Antarctic Peninsula underlain by weaker mantle. Current global-scale GIA models are  
35 unable to predict our observed changes in Late Holocene RSL. Complexities in Earth structure and  
36 neoglacial history need to be taken into consideration in GIA models used for correcting modern  
37 satellite-based observations of ice-mass loss.

38

## 39 **1. Introduction**

40 As early as Nichols (1960), the nature of relative sea-level (RSL) change across Antarctica was  
41 interpreted to reflect glacial isostatic adjustment (GIA) in response to the decay of the LGM ice sheets.  
42 Initial attempts at fitting observations of RSL change to model predictions of GIA in Antarctica used a  
43 relatively strong Earth rheology (Pallas et al., 1997; Zwartz et al., 1998; Bassett et al., 2007). In addition,  
44 many of these initial GIA studies assumed that the ice sheet experienced a continuous demise with few  
45 if any readvances (and subsequent retreats) through the Holocene (e.g. ANT3, Nakada and Lambeck,

46 1988; ICE-5G, Peltier, 2004; W12, Whitehouse et al., 2012b). These initial GIA model predictions (Pallas  
47 et al., 1997; Zwartz et al., 1998; Bassett et al., 2007; Whitehouse et al., 2012b) appear to fit the sparse  
48 RSL observations available from the continent and its neighboring islands (Nichols, 1960; Pallas et al.,  
49 1997; Hall and Denton, 1999; Baroni and Hall, 2004; Roberts et al., 2011; Simkins et al., 2013b).  
50 However, both the existence of a strong Earth rheology and the assumption of no Holocene ice  
51 readvances have been challenged by recent studies showing local ice advances in parts of the northern  
52 Antarctic Peninsula (Smith, 1982; Hansom and Flint, 1989; Hjort et al., 1997; Hall, 2007; Hall et al., 2010).

53         Recent warming across the Antarctica Peninsula and Southern Ocean has brought about a  
54 natural experiment in which to test the existence of a relatively stiff and strong rheology beneath the  
55 Antarctic Peninsula. Remote sensing along with historical records have been used to reconstruct the  
56 amount of ice-mass loss over historical time periods (Nield et al., 2012; 2014; Zhao et al., 2017). These  
57 reconstructions coupled with GPS observations of uplift effectively constrain the Earth structure  
58 beneath the Antarctic Peninsula (Nield et al., 2014; Zhao et al., 2017). In particular, Nield et al. (2014)  
59 show that the large increase in uplift rates recorded in the GPS data since ice-shelf collapse in 2002  
60 cannot be explained by elastic deformation alone but reflect a visco-elastic Earth response.  
61 Furthermore, the amount of visco-elastic response suggests that some regions of the Antarctic Peninsula  
62 are underlain by a much weaker rheology than early and global GIA models have suggested (Ivins et al.,  
63 2011; Nield et al., 2014).

64         Additional work focused on reconstructing the history of the Antarctic Peninsula Ice Sheet has  
65 also provided evidence for late Holocene ice-sheet oscillations (Hjort et al., 1997; Hall et al., 2010). In  
66 addition, GPS observations in areas far removed from ice shelves undergoing recent collapse have found  
67 that post-LGM ice loss alone cannot explain current rates of rebound but require late Holocene ice-mass  
68 changes (Bradley et al., 2015; Wolstencroft et al., 2015). Only recently have GIA-models considered the  
69 possibility of Holocene ice-sheet oscillations (Ivins et al., 2011). Such oscillations could result in

70 observable changes in the rate of RSL change through the Holocene if portions of the Antarctic  
71 Peninsula are underlain by a relatively weak Earth structure. Such changes in the rate of RSL fall have  
72 been documented in the South Shetland Islands (Hall, 2010; Watcham et al., 2011; Simms et al., 2012),  
73 which might be expected to have a weaker rheology given their location overlying an active subduction  
74 zone, but have yet to be documented for the Antarctic Peninsula proper.

75         The purpose of this study is to use optically-stimulated luminescence (OSL) ages of raised  
76 beaches to reconstruct a new RSL record from the northern Antarctic Peninsula continental margin in an  
77 area where prior GPS work has documented rapid uplift suggestive of a relatively weak rheology. If the  
78 Antarctic Peninsula is underlain by a weaker-than-average Earth structure and its ice sheet has been  
79 subject to Holocene oscillations, one would expect to find evidence for variable rates of RSL change  
80 during the late Holocene rather than the monotonic decrease predicted by simple post-LGM ice retreat.  
81 We test this hypothesis. Furthermore, after correcting our new RSL record for GIA-induced changes in  
82 the sea-surface height and assuming minimal influences from steric impacts on the Holocene record of  
83 sea-level change, we compare our new rate of Holocene uplift to recent GPS (1998-present)  
84 measurements of uplift at Palmer Station along the northern Antarctic Peninsula. This comparison is  
85 used to determine if recent rates of RSL fall are unprecedented in the late Holocene.

## 86 **2. Background**

### 87 *2.1 Late Holocene Sea Levels and Rates of RSL Change*

88         One of the best millennial-scale archives of glacial isostatic adjustment is Holocene RSL records.  
89 Relative sea-level reconstructions for the western Antarctic Peninsula are available for the South  
90 Shetland Islands at the northern tip of the Antarctic Peninsula (John and Sugden, 1971; Bentley et al.,  
91 2005; Hall, 2010; Watcham et al., 2011; Simms et al., 2012) and in Marguerite Bay to the south (Nichols,  
92 1960; Bentley et al., 2005; Hodgson et al., 2013; Simkins et al., 2013b), leaving a 600+ km stretch of

93 coast with little to no constraints on Holocene sea-level changes (Fig. 1). Along the eastern Antarctic  
94 Peninsula the only sea-level indicators are found at Beak Island (Roberts et al., 2011) and James Ross  
95 Island (JRI) (Ingolfsson et al., 1992; Hjort et al., 1997) (Fig. 1).

96 Relative sea-level reconstructions from the South Shetland Islands record a recent sea-level fall  
97 on the order of 6 m within the last 300-500 years at a rate possibly as high as 12.5 mm/yr preceded by  
98 an overall 10-12 m fall in sea level since 6 ka (Bentley et al., 2005; Hall, 2010; Watcham et al., 2011;  
99 Simms et al., 2012). The rapid RSL changes within the South Shetland Islands (Hall, 2010; Watcham et  
100 al., 2011) have been attributed to the relatively weak rheology beneath the active arc (Simms et al.,  
101 2012). Sea-level records from Marguerite Bay show a fall in sea level from an approximate highstand of  
102 20-22 m at 7-7.5 ka to <5 m around 2-2.5 ka (Bentley et al., 2005; Hodgson et al., 2013; Simkins et al.,  
103 2013b). This fall may have been preceded by a rise in RSL contributing to the formation of a prominent  
104 scarp within northern Marguerite Bay (Simkins et al., 2013b). Since 2-2.5 ka, sea levels within  
105 Marguerite Bay have fallen at a rate of less than 1.4 mm/yr (Simkins et al., 2013b).

106 The records from the eastern Antarctic Peninsula are sparser, with three sea-level index points  
107 from Beak Island (Roberts et al., 2011) and two sets of marine/beach deposits from northern JRI  
108 (Ingolfsson et al., 1992; Hjort et al., 1997) (Fig. 1). The age-elevation relationships of the three indices  
109 from Beak Island are precisely established from isolation basins (Roberts et al., 2012). This work  
110 suggests rates of RSL fall decreased from 3.9 mm/yr between 8 ka and 6.9 ka to 2.1 mm/yr between 6.9  
111 ka and 2.9 ka, leveled off to 1.6 mm/yr between 2.9 ka and 1.8 ka, and further decreased to 0.29 mm/yr  
112 over the last 1.8 ka. Constraints on rates of RSL changes from the two sets of raised marine features  
113 found on JRI (Hjort et al., 1992) are not as clear. At the first site, Brandy Bay, two sets of raised beaches  
114 are found, with a higher, more weathered set of beaches at elevations from 30-18 m and a lower, better  
115 preserved, set of beaches at less than 16 m (Ingolfsson et al., 1992; Hjort et al., 1997). At a second site  
116 on JRI, The Naze, the lower set of beaches is found at elevations less than 18 m (Hjort et al., 1997). In

117 addition to the beaches at The Naze, cliff exposures reveal an 18 m thick succession of late Holocene  
118 glacial-marine and shoreface deposits with *in situ* mollusks. The succession places sea levels higher than  
119 18 m around 7.5 ka (Hjort et al., 1997). Hjort et al. (1997) therefore assign the older beaches with an  
120 upper limit of 30 m to an age of 7.5 ka and the lower beaches with an upper limit of 16-18 m to an age  
121 of 4.2-4.5 ka based on ages from *in situ* mollusks from another lower section of glacial marine deposits  
122 close to the lower raised beaches within Brandy Bay. The stratigraphy and correlations provide a well-  
123 documented framework for Holocene sea-level changes but the elevation-age relationship cannot be  
124 directly confirmed.

## 125 *2.2 Recent Changes across the Antarctic Peninsula*

126 The Antarctic Peninsula is one of the most rapidly warming places on the planet (Hansen et al.,  
127 1999; Vaughan et al., 2003). Recent warming has brought dramatic changes to the region including an  
128 increase in ice melting recorded in ice core data (Abram et al., 2013), the disappearance of ice shelves  
129 (Vaughan and Doake, 1996; Rott et al., 1996; Hodgson et al., 2011), changes in ocean circulation  
130 (Jourdain et al., 2017), the retreat of tidewater glaciers (Cook et al., 2005) and sea ice (Cavalieri and  
131 Parkinson, 2008; Jourdain et al., 2017), and changes in regional ecology and ecosystems (Moline et al.,  
132 2008; Montes-Hugo et al., 2009; Mintenbeck and Torres, 2017; Amesbury et al., 2017). The retreat of  
133 glaciers due to both warming and the breakup of ice shelves reflects an increase in the regional rate of  
134 mass loss (Rignot et al., 2008). This decrease in mass was accompanied by an increase in uplift rates  
135 recorded in GPS observations across the Antarctic Peninsula (Thomas et al., 2011; Nield et al., 2014).  
136 This acceleration in uplift is more pronounced in the northern Antarctic Peninsula than the central  
137 Antarctica Peninsula (Thomas et al., 2011; Nield et al., 2014). For example, GPS observations from  
138 Palmer Station record a 110-fold increase in uplift rates following the demise of the Larsen B Ice Shelf in  
139 2002 (Thomas et al., 2011; Nield et al., 2014) while farther south along the Antarctic Peninsula at  
140 Rothera Station, uplift rates increased by a factor of less than 5 (Thomas et al., 2011). Part of these

141 differences can be attributed to differences in the local magnitude of grounded ice loss but part has  
142 been attributed to differences in the rheology of the underlying earth (Zhao et al., 2017).

### 143 *2.3 Role of other drivers of sea-level change*

144 In addition to GIA, rock uplift, and ocean volume changes, steric changes such as changing ocean  
145 temperatures and changes in wind patterns can also drive relative sea-level changes. Over the last 50  
146 years, ocean temperatures have warmed nearly 1°C within the Bellingshausen and Amundsen Seas  
147 (Meredith and King, 2005). This warming along the Antarctic Peninsula is seen to be a response to  
148 global climate variability including changes in the Atlantic Multidecadal Oscillation (Li et al., 2014). Sea-  
149 surface temperatures across the Antarctic Peninsula have also changed throughout the late Holocene  
150 with the amplitude of oscillations reaching as much as 1.8°C over the last 2 ka (Shevenell et al., 2011).  
151 However, such temperature changes are unlikely to have caused sea-level variations of more than a few  
152 tens of cm (Landerer et al., 2007). For example, along the Pacific coasts of North and South America,  
153 local ocean temperature increases of up to 2-5°C during El Nino years brought about only 20 to 30 cm of  
154 sea-level change (Hamlington et al., 2015). Some of these same studies, although not specifically  
155 focused on the western Antarctic Peninsula, only show a few cm's of sea-level variability across the  
156 Southern Ocean near the western Antarctica Peninsula (Hamlington et al., 2015). As for wind changes,  
157 based on the analysis of tide-gauge data at Vernadsky Station approximately 50 km south of Palmer  
158 Station, Aoki (2002) found less than 10 cm of sea-level variability due to changes in winds associated  
159 with the Southern Hemisphere Annular Mode, with a mean increase in wind speeds of 1 m/s increasing  
160 sea levels by only 1 cm.

161

### 162 *2.4 Evidence for late Holocene ice-changes across the western Antarctic Peninsula*

163 Evidence of late-Holocene advances and retreats within the western Antarctic Peninsula are  
164 found both in the terrestrial and marine record. Terrestrial records of glacial/ice sheet changes near our  
165 field site on Torgerson Island include observations of floral development on the rock-exposed headlands  
166 near Palmer Station (Smith, 1982) as well as reworked material within tills (Hall et al., 2010). Although  
167 no terminal moraines have been identified, a distinct decrease in the development and changes in the  
168 types of mosses and lichens suggest the ice extended approximately 150 m farther seaward of its 1977  
169 AD limits (the ice has continued to retreat since 1977) within the last millennium (Smith, 1982). The  
170 remnants of what appeared to be moss overridden by the ice dated to 0.54 ka (0.67 ka to 0.32 ka)  
171 suggesting the ice advanced sometime after this date (average of 3 ages recalibrated from Smith, 1982).  
172 In addition to this advance, Hall et al. (2010) found evidence of a more landward position (less ice) of the  
173 glacier near Palmer Station within the late Holocene. Mosses incorporated into the modern moraines  
174 near Palmer Station suggest ice-free areas existed beneath the present glacier around 0.7-0.97 ka  
175 indicating a retreat of the glacier prior to its advance suggested by Smith (1982). Furthermore, other  
176 mosses within the banks point to other potential periods of less extensive ice around 3.7 and 5.6 ka (Hall  
177 et al., 2010).

178 Outside of the region around our study area, terrestrial evidence for late Holocene ice-sheet  
179 oscillations have been found on the South Shetland Islands (Curl, 1980; Clapperton and Sugden, 1988;  
180 Birkenmajer, 1998; Hall, 2007; Simms et al., 2012), Brabant Island (Hansom and Flint, 1989), and James  
181 Ross Island (Hjort et al., 1997). Of the records on the South Shetland Islands, the best dated is probably  
182 that of Hall (2007) who obtained 28 radiocarbon ages within a well-developed moraine on King George  
183 Island. The ages suggest the moraine formed from an advance less than 650 years ago that was  
184 preceded by less extensive ice present sometime after ~3.5 ka (Hall, 2007). Hansom and Flint (1989)  
185 and Hjort et al. (1997) both dated reworked mollusk shells within moraines suggesting an advance  
186 sometime around 5 ka.



187 Marine records from the fjords across the western Antarctic Peninsula also point to glacial and  
188 climatic fluctuations throughout the late Holocene. Direct records of an ice advance leading up to the  
189 Little Ice Age at approximately 0.2 ka are recorded in cores from Barilari Bay approximately 130 km  
190 south of Palmer Station (Christ et al., 2015). Proxy records from the Palmer Deep 25 km south of Palmer  
191 Station point to almost 1.3°C warming of sea-surface temperatures between 1.8 ka and 1.6 ka with a  
192 similar magnitude cooling between 0.5 ka and 0.1 ka with no fewer than 8 additional but smaller  
193 amplitude sea-surface temperature changes since 1.8 ka (Shevenell et al., 2011). Several other proxy  
194 records of climatic changes have been retrieved from marine sediments within the Palmer Deep  
195 (Leventer et al., 1996; Shevenell and Kennett, 2002) and elsewhere across the western Antarctic  
196 Peninsula (Heroy et al., 2008; Allen et al., 2010; Yoon et al., 2010; Reilly et al., 2016; Kim et al., 2018) all  
197 pointing to climatic and potentially glacial fluctuations through the late Holocene.

## 198 *2.5 Field Site*

199 Our new RSL site at Torgersen Island is located along the western Antarctic Peninsula within the  
200 Palmer Archipelago on the southern side of Anvers Island (Figs. 1 and 2). It is 285 km south and 375 km  
201 north of the closest RSL records for the western Antarctica Peninsula in the South Shetland Islands and  
202 Marguerite Bay, respectively. It is located less than 1 km to the west of the Palmer Station GPS site,  
203 which itself lies on a small peninsula extending from Anvers Island (Fig. 2). The region consists of  
204 isolated rock drumlins and other glacially-carved landforms covered in a veneer of late Holocene till,  
205 outwash, and raised marine features (Hall et al., 2010). Anvers Island partly shields the Torgersen Island  
206 region from the dominant swell originating in the southern Pacific Ocean and traveling through the  
207 Bellingshausen Sea (Fig. 1).

208 Although Torgersen Island is located on the Bellingshausen Sea, the region is only separated  
209 from the Weddell Sea and the former location of the Larsen B Ice Shelf by a narrow spine of mountains

210 comprising the northern Antarctic Peninsula (Fig. 1). As such it is located less than 100 km from the  
211 former Larsen B Ice Shelf and within the influence of increased uplift rate due to ice flow acceleration  
212 following the recent demise of the ice shelf (Thomas et al., 2011; Nield et al., 2014).

### 213 **3. Methods**

#### 214 *3.1 Basics of OSL dating*

215           Optically stimulated luminescence (OSL) dating determines the last exposure of mineral grains  
216 to sunlight. The age range is from recent decades to 200,000 years ago with an age-uncertainty of 5-  
217 10%. New methodologies promise an extension of the upper age limit to 1 million years (e.g. Porat et al.,  
218 2009). Bøtter-Jensen et al. (2003), a review by Rhodes (2011), and a series of dedicated contributions in  
219 the recently published Encyclopedia of Scientific Dating Methods (Rink and Thompson, 2013) give a  
220 detailed description of the OSL method. OSL dating works on the principle that radiation – from U, Th, K,  
221 and from cosmic rays – ionizes atoms within silicate minerals like quartz and feldspar. The freed  
222 electrons become trapped at light sensitive crystal defects. When exposed to sunlight, the electrons are  
223 released from the traps. In returning to their original states they emit luminescence and the mineral is  
224 reset. Upon burial trapped electrons accumulate again, and their number is proportional to the burial  
225 time and the radiation exposure, often termed the “dose”. The rate of irradiation, the “dose rate,” can  
226 be calculated from the cosmic flux as well as the U, Th, and <sup>40</sup>K concentrations of the surrounding  
227 materials. The OSL signal is proportional to the dose and can be measured by exposing the mineral to  
228 light in a controlled setting. An age since burial can be determined by dividing the dose by the dose rate.  
229 The lower age limit of the methodology is determined by the smallest measurable signal. The upper age  
230 limit depends on the saturation range of the sample, where the signal shows only little increase with  
231 dose. Typically this procedure is conducted on sand-sized quartz grains (Murray and Wintle, 2003), but

232 recent advances have allowed for the use of OSL on cobble surfaces (Simms et al., 2011; Simkins et al.,  
233 2016).

### 234 *3.2 OSL Sampling*

235 Torgersen Island as well as nearby Litchfield Island and Biscoe Point were visited in the austral  
236 fall of 2010 (Figs. 1 and 2). The deposits from Torgersen and Litchfield Islands were described and  
237 surveyed using a survey-grade Trimble GPS. However, the samples from Biscoe Point were surveyed  
238 using an altimeter due to difficulties associated with the GPS equipment in the field. Elevations were  
239 initially calculated relative to the water level elevation at the time of the survey. The offset between the  
240 water level elevation at the time of the survey and mean sea level was corrected for using the tide  
241 gauge located at Palmer Station. Cobbles for optically stimulated luminescence (OSL) dating were  
242 collected under a light-proof tarpaulin to avoid sunlight exposure (Simms et al., 2011). Samples were  
243 taken from raised beaches at 5.0 and 7.2 m above modern sea levels (Simkins et al., 2015) as well as the  
244 modern beaches on nearby Litchfield Island (0.5 m above sea level) and Biscoe Point (~2.0 m above sea  
245 level). The latter two sites were sampled in order to determine if modern beaches gave an OSL age of  
246 zero.

### 247 *3.3 OSL Ages*

248 In the laboratory the outside 1 mm of the undersides of the cobbles was isolated using a Buehler  
249 Isomet 1000 precision saw. These thin rock slices were crushed lightly using a ceramic mortar and  
250 pestle to disaggregate the constituent mineral crystals (Simkins et al., 2016). The crystal segregates  
251 were sieved to isolate grains between 63  $\mu\text{m}$  and 250  $\mu\text{m}$ . Following treatment with 3.75% HCl and 27%  
252  $\text{H}_2\text{O}_2$ , the isolated grains underwent density separations of 2.62 and 2.75  $\text{g}/\text{cm}^3$  to extract the quartz  
253 fraction. The quartz fraction was further etched with 48% HF for 40 minutes. Approximately 100-200

254 grains (3 mm aliquots) were prepared on sample carriers using a silicone oil spray. Sample carriers were  
255 cleaned as described by Simkins et al. (2013a) and selected for negligible intrinsic signals.

256 The OSL measurements were carried out using a Risø TL/OSL-DA-15 Reader with a built-in  
257  $^{90}\text{Sr}/^{90}\text{Y}$  beta source. Blue LEDs (470 nm, 31 mW/cm<sup>2</sup>) and IR LEDs (875 nm, 110 mW/cm<sup>2</sup>) were used  
258 for optical stimulation and infrared stimulation, respectively. OSL signals were detected in the UV-  
259 window (Hoya U340, 7.5 mm, 340 nm peak) with 1-s counting intervals. Heating rate used was 5°C/s.  
260 The single-aliquot regenerative dose (SAR) procedure was used for determining the equivalent doses  
261 (Murray and Wintle, 2000; Wintle and Murray, 2006) with high-temperature stimulation (Murray and  
262 Wintle, 2003) and a post-IR blue sequence (Wallinga, 2002; Duller, 2003) following the measurement  
263 protocol outlined in Simkins et al. (2013a, b). Aliquots for dose calculations were selected according to  
264 the reliability test recommended by Wintle and Murray (2006) and described in detail by Simkins et al.  
265 (2015). The extracted quartz was dim and aliquots were considered to be reliable if their recuperation  
266 was <10%, recycling ratios <20%, and dose deviation <25%. We used the common age model (Galbraith  
267 et al., 1999) for final age determinations.

### 268 *3.4 GIA Modeling*

269 Relative sea-level change is not only a function of vertical land motion (as measured by GPS) but  
270 also a function of changes in the height of the sea surface. We used a global GIA model to estimate the  
271 change in sea surface height (SSH) attributed to changes in water volume and the gravitational  
272 components of GIA in order to isolate what portion of the RSL signal was due to local land motion  
273 assumed to be controlled by ice mass changes, without explicitly modelling those ice-mass changes. The  
274 sensitivity of the SSH signal to local ice-mass change is discussed below. Sea surface heights can also be  
275 influenced by steric (water-temperature) changes and wind-driven stresses. However, as steric and  
276 wind-driven changes are only on the order of a few tens of cm's (Aoki, 2002; Landerer et al., 2007;

277 McKay et al., 2011; Hamlington et al., 2015), we assumed they were less than a few 10's of cm over the  
278 time scales of our RSL reconstructions.

279 We simulated the GIA process following the methods of Whitehouse et al. (2012b), using the ice  
280 model of Whitehouse et al. (2012a) without the Antarctic Peninsula adjustment (Whitehouse et al.,  
281 2012b) for Antarctica and ICE-5G for the Northern Hemisphere (Pelter, 2004). In order to determine  
282 what impact a local ice-sheet oscillation may have had on the SSH, we also considered three modified  
283 ice-sheet models. These modified ice-sheet models were constructed by decreasing the amount of ice  
284 within the original Whitehouse et al. (2012a) model to 90% of its original thickness at 1 ka and  
285 increasing it to 101%, 105%, and 110% of its original thickness at 0.5 ka. These modifications were  
286 applied to the Antarctic Peninsula ice sheet north of 68.5° S latitude. Our GIA model predictions account  
287 for the impacts of migrating shorelines, marine-based ice, and rotational feedback (Kendall et al., 2005).  
288 We assumed a spherically symmetric, self-gravitating Maxwell viscoelastic Earth structure, but in order  
289 to reflect suggestions that different regions of Antarctica may be underlain by different Earth rheology  
290 (van der Wal et al., 2015) we considered 24 different Earth models with lithospheric thicknesses of 46,  
291 71, 96, and 120 km, upper mantle viscosities of 0.05, 0.08, 0.1, 0.2, 0.3, 0.5, and  $0.8 \times 10^{21}$  Pa s, and  
292 lower mantle viscosities of 3, 10, and  $20 \times 10^{21}$  Pa s. Our GIA model has an inherent resolution or  
293 truncation degree of 256. Lower mantle viscosities of 3 and  $20 \times 10^{21}$  Pa s were only used in conjunction  
294 with the Earth model that has a lithospheric thickness of 96 km and upper mantle viscosity of  $0.3 \times 10^{21}$   
295 Pa s. Although the upper mantle viscosities used are slightly higher ( $10^{19}$  versus  $10^{18}$  Pa s) than those  
296 suggested by Nield et al. (2014), our selection of upper mantle viscosities spanning 2 orders of  
297 magnitude result in less than 0.2 mm/yr of difference to our predictions of sea surface height change  
298 over the last 2 ka (see below).

299 The GIA model allows us to estimate GIA-driven changes to sea surface height, and the  
300 deformation of the sea floor at Torgersen Island, during the mid-to-late Holocene. Although the

301 magnitude of solid-Earth deformation is highly sensitive to the Earth model, the sea surface component  
302 is relatively insensitive to both the choice of Earth model and the potential local ice sheet oscillations  
303 (see results). We therefore use the mean of the 96 model predictions (24 Earth models x 4 ice models)  
304 to correct the RSL observations for sea-surface height change, yielding a data-driven estimate for solid-  
305 earth deformation during the late Holocene, which may be directly compared with GPS-derived  
306 measurements of contemporary deformation. Two standard deviations (rounded up) of the 96 model  
307 predictions is used to quantify the error associated with model uncertainties.

## 308 **4. Results**

309

### 310 *4.1 Ages*

311

312 The ages from Torgersen Island presented here were previously reported as part of a  
313 compilation of Antarctic raised beach ages (Simkins et al., 2015). The samples from Litchfield Island and  
314 Biscoe Point at elevations of 0.5 m and ~2.0 m, respectively, contained no natural dose, suggesting  
315 recent exposure and a “zero” age for the modern beach (Table 1). Two ages were obtained from the  
316 Torgersen Island beach at 7.2 m (Table 1). These ages are 1480 and 2180 years with 2-sigma errors of  
317 200 and 680 years, respectively. Although they fall within error of one another, the age with the largest  
318 error bar, due to high aliquot measurement scatter (i.e. overdispersion), is older by 700 years. We  
319 therefore use a weighted mean based on their errors (Taylor, 1997) to determine an age of  $1540 \pm 190$   
320 years for our RSL calculations. The single age from the 5.0 m beach ridge on Torgersen Island was 790  
321 years with a 2-sigma error of 180 years.

### 322 *4.2 Rates of Holocene Sea-Level Change*

323 The two beach ridges from Torgersen Island have the same geomorphic expression – low  
324 amplitude ridge fronting a broad depositional flat bench (Fig. 2). Following Fretwell et al. (2010), we  
325 therefore assume that they formed at similar elevations with respect to sea level at the time of their  
326 formation. Although no ground-penetrating radar is available from this site, the morphology of a flat  
327 bench is suggestive of a depositional plain similar to the strandplain deposits reported from the South  
328 Shetland Islands by Lindhorst and Schutter (2014) rather than a storm-built berm (Butler et al., 1999).  
329 Thus for calculating rates of RSL change between the formation ages of these two beach ridges, we use  
330 the following expression:

$$331 \quad dRSL/dt = (E_{br1} - E_{br2}) / (T_{br1} - T_{br2}) \quad (1)$$

332 where  $E_{br1}$  and  $E_{br2}$  are the elevation of the beach ridges in meters and  $T_{br1}$  and  $T_{br2}$  are their ages in  
333 years. The error was determined using the following expression:

$$334 \quad E = (1 / (T_{br1} - T_{br2})) * (\delta E_{br1}^2 + \delta E_{br2}^2 + (dRSL/dt)^2 * (\delta T_{br1}^2 + \delta T_{br2}^2))^{0.5} \quad (2)$$

335 where  $\delta E$  and  $\delta T$  are the errors in the elevations and ages of the beach ridges. Beach-ridge elevation  
336 errors were added in quadrature and accounted for errors in the GPS (<0.1 m), 2 standard deviations of  
337 the average beach ridge elevations surveyed along strike (<0.3 m), and 2 standard deviations of the  
338 average tidal level during the time of the survey (<0.1 m) for a total error of 0.3 m. The rate of RSL fall  
339 between the 7.2 and 5.0 m beaches is  $3.0 \pm 1.2$  mm/yr (Table 2).

340 We were not able to survey the elevation of the modern beach on Torgersen at the time of our  
341 OSL collection. However, a recent topographic survey and published map places the modern beach at  
342 around 1 m and well below 2 m (Lorenz and Harris, 2014). In addition, we did survey the elevations of  
343 modern beaches on nearby Litchfield Island and Biscoe Point, both of which produced OSL ages of 0 or  
344 modern (Table 1). The modern beach on Litchfield Island is found at an elevation of 0.5 m (Table 1),  
345 while the modern beach surveyed on nearby Biscoe Point is found at an elevation of ~2.0 m (based on

346 altimeter not GPS). These elevations are similar to surveyed modern beaches in other parts of the  
347 Antarctic Peninsula, which are found at elevations of less than 2 to 3 meters (Bentley et al., 2005; Hall,  
348 2010; Simms et al., 2011; Fretwell et al., 2011). Their variability likely represents local differences in  
349 fetch, grain size, and shallow water bathymetry – all of which impact beach heights. We therefore  
350 assign an elevation of the modern-equivalent beach on Torgersen Island to  $1.0 \pm 1.0$  m. Using Eqs. 1 and  
351 2 from above yields a rate of RSL fall of  $5.1 \pm 1.8$  mm/yr since 0.79 ka (Table 2).

#### 352 *4.3 GIA-Induced Sea-Surface Corrections*

353 Our Holocene estimates of rates of relative sea-level change cannot be directly compared with  
354 the GPS uplift rates because RSL is a function of more than simply the amount of vertical land motion.  
355 However, using a GIA model we estimate the component of RSL change associated with changes in the  
356 sea-surface height, and by correcting for this minimize the expected differences between the two types  
357 of measurements. Depending on the Earth model, the deglaciation model of Whitehouse et al. (2012a)  
358 yields a sea-surface (i.e. non-solid earth) rate component of between 0.38 and 0.21 mm/yr for the time  
359 period between 1.54 ka and 0.79 ka and between 0.22 and 0.04 mm/yr for the time period from 0.79 ka  
360 to the present, where the positive values indicate gradual SSH rise over these periods (Figs. 3A and 3B).  
361 Accounting for possible ice-sheet oscillations over the last 2 ka increases those SSH rates of change by  
362 less than 0.02 mm/yr for the time period between 1.54 and 0.79 ka and between 0.01 and -0.03 mm/yr  
363 (negative values denote a sea-surface fall) for the time period between 0.79 and the present (Figs. 3C  
364 and 3D; the value of -0.03 mm/yr although not shown on Fig. 3D occurs within the predictions using the  
365 ice-sheet model with only a 1% increase in ice at 0.5 ka). Combining these potential variations in the  
366 SSH results in a total SSH correction of  $0.3 \pm 0.1$  and  $0.2 \pm 0.1$  mm/yr for the time periods of 1.54 to 0.79 ka  
367 and 0.79 ka to the present, respectively. Correcting our RSL estimates for GIA-induced SSH changes  
368 yields uplift rates of  $3.3 \pm 1.2$  mm/yr between 0.79 ka and 1.54 ka and  $5.3 \pm 1.8$  mm/yr since 0.79 ka and  
369 (Table 2; Fig. 4).



370 Prior to 8 ka, GIA-induced sea-surface height changes are predicted to have kept pace with uplift  
371 rates for several millennia (Fig. 5), reflecting the influence of meltwater input from the decaying  
372 northern hemisphere ice sheets at this time. However, during the late Holocene, rates of GIA-induced  
373 sea-surface height change are predicted to have been minor in comparison to the rates of RSL fall over  
374 the same period and were never greater than 0.5 mm/yr over the last 2.5 ka (Table 2, Fig. 5). Predictions  
375 for sea-surface height changes vary little across the Antarctica Peninsula (not shown) and thus variations  
376 in the rate of RSL fall largely reflect differences in the rate of solid earth deformation.

## 377 **5.0 Discussion**

### 378 *5.1 Changes in Holocene Rates of RSL Fall*

379 Although the rates of RSL fall derived from the 7.2- to 5.0-m beaches and the 5.0-m to modern  
380 beach ridges overlap within error, the central values suggest an increase in the rate of RSL fall by  $2.1$   
381  $\pm 2.2$  mm/yr after 0.79 ka (Table 2). This increase becomes marginally smaller after correcting for sea-  
382 surface height changes to obtain uplift rates ( $2.0 \pm 2.2$  mm/yr). The sign of this change is opposite to the  
383 decrease in rate that would be expected if the late Holocene record of RSL and uplift was dominated by  
384 post-LGM isostatic rebound alone. The potential increase may represent the solid-earth response to the  
385 late Holocene ice retreat to smaller-than-present margins that is documented for the Marr Ice  
386 Piedmont, which lies within 2 km of our beach sites (Hall et al. 2010). Hall et al. (2010) found reworked  
387 moss dating to 0.7-0.97 ka along with reworked marine shells within a moraine recently exposed due to  
388 recent warming in the Antarctic Peninsula (Hall et al., 2010). This episode of late Holocene ice loss may  
389 have been in response to warmer sea-surface temperatures recorded in the region (Shevenell et al.,  
390 2011). However, more RSL data points are needed to constrain the exact timing of the RSL rate changes.  
391 Such sensitivity of the solid earth to late Holocene glacial retreats would support assertions of a  
392 relatively weak underlying upper mantle (Nield et al., 2012; 2014).

393 A Late Holocene retreat to smaller-than-present margins had to be followed by an ice advance  
394 to the pre-1950 glacial margins sometime within the last 800 years. Smith (1982) provides evidence in  
395 the form of the density and types of mosses and lichens present near Palmer Station of a glacial advance  
396 sometime after 0.54 ka. Such an advance may have dampened any ongoing solid-earth response to the  
397 0.7-0.97 ka retreat documented by Hall et al. (2010); which is weakly shown in our GIA modeling (Fig. 5).  
398 Indeed, Nield et al. (2014) suggest that initiation of the viscoelastic response to local ice mass change  
399 may be within a few months in this region, leading us to hypothesize that RSL change (largely reflecting  
400 changes in uplift rate) during the late Holocene may have been much more variable than is reflected by  
401 the time-averaged RSL rates derived from the Holocene beach ridges on Torgersen Island. In particular,  
402 rates of RSL fall may have been instantaneously greater than those recorded by the beach ridges, which  
403 tend to provide averages for periods during the late Holocene.

#### 404 *5.2 RSL versus GPS Uplift Rates*

405 The late Holocene average uplift rates from 0.79 ka to the present at Torgersen Island, derived  
406 by correcting observed RSL rates for the signal due to sea surface height change, are approximately  
407 5 mm/yr greater than the pre-2002 GPS-observed uplift rates measured at Palmer Station (1998-2002;  
408  $0.08 \pm 1.87$  mm/yr; Thomas et al., 2011), and only slightly lower than the rates measured since the  
409 breakup of the Larsen B Ice Shelf in 2002 ( $6.6 \pm 2.1$  mm/yr based on data from 2002-2013 by Nield et al.,  
410 2014;  $8.75 \pm 0.64$  mm/yr based on data from 2002-2010 by Thomas et al., 2011). Nield et al. (2014)  
411 demonstrated that the rapid change in GPS-observed uplift rates between pre- and post-2002 could not  
412 be explained by an elastic-only response to local ice loss. The authors concluded that the GPS must also  
413 be recording a viscoelastic response and constrained the upper mantle in this region to relatively weak  
414 viscosities of  $6 \times 10^{17}$ - $2 \times 10^{18}$  Pa s. The large difference between late Holocene RSL-derived uplift rates  
415 (3.3 to 5.1 mm/yr) and pre-2002 GPS-observed uplift rates ( $<0.1$  mm/yr) suggests that either glacial  
416 isostatic adjustment associated with post-LGM ice loss has decreased significantly since 0.79 ka or the

417 RSL-derived rates reflect a localized response of the weak upper mantle to late Holocene advances and  
418 retreats, which had either decayed by 1998 or was reduced by increased accumulation following the LIA  
419 (Nield et al., 2012). This difference in pre-2002 and Holocene rates further supports a strong RSL  
420 sensitivity to late Holocene ice mass changes and a weaker relationship between late-Holocene RSL and  
421 post-LGM deglaciation.

### 422 *5.3 Implications for GIA and ice-sheet models and estimates of ice-sheet mass balance changes*

423 The relatively weak Earth structure beneath parts of the Antarctic Peninsula implied by recent  
424 GPS observations is also reflected in the rates of late Holocene RSL change observed across the Antarctic  
425 Peninsula. If this result is robust, it implies that Holocene records of RSL generated along these parts of  
426 the Antarctic Peninsula may not be as effective a tool for constraining the configuration of the LGM  
427 Antarctic ice sheet as they are across the northern hemisphere. This is important, not only because GIA  
428 model comparisons to RSL data play an important role in efforts to reconstruct past ice sheet history  
429 (e.g. Ivins and James, 2005; Whitehouse et al., 2012a; b), but also because accurate GIA predictions are  
430 therefore needed to interpret gravity-based estimates of ice loss (Shepherd et al., 2012; King et al.,  
431 2012). Our findings support earlier studies suggesting neoglacial advances can strongly influence  
432 modern rates of uplift (Ivins et al., 2000). Such effects must be included in future GIA models and  
433 accounted for in estimates of ice mass loss based on satellite gravity measurements (Ivins et al., 2011).

## 434 **5. Conclusions and Future Prospects**

435 The rate of relative sea-level fall at Torgersen Island near Palmer Station in the Antarctic  
436 Peninsula increased from  $3.0 \pm 1.2$  mm/yr to  $5.1 \pm 1.8$  mm/yr around 0.79 ka broadly contemporaneous  
437 with glacial retreat within a nearby ice piedmont. The sensitivity of these Holocene sea-levels to ice-  
438 mass changes supports GPS-based assertions of a relatively weak upper mantle beneath this parts of the  
439 Antarctic Peninsula. Furthermore, the rate of Holocene uplift at Torgersen Island, derived by correcting

440 RSL rates for sea-surface elevation changes and assuming negligible steric effects ( $5.3 \pm 1.8$  mm/yr), far  
441 exceeds the pre-2002 GPS-derived uplift rates recorded at Palmer Station but is similar to the rates  
442 experienced since the breakup of the Larsen B Ice Shelf in 2002. The sensitivity of Holocene RSL rates  
443 near Palmer Station to late Holocene ice retreats suggests that these records are not recording post-  
444 LGM ice collapse but more recent ice changes, and more data are needed to constrain not only the RSL  
445 record from sites with a weak mantle in Antarctica, but also their Holocene ice history. Thus their use in  
446 constraining GIA models of the LGM ice sheet should be revisited and corrections applied to satellite  
447 data to determine ongoing mass loss should be updated accordingly.

448

#### 449 **Acknowledgements**

450 The authors would like to thank Marissa Goerke for sharing the tide-gauge data from Palmer Station and  
451 Colin Harris for answering questions about the mapping of Torgersen Island. This project benefited from  
452 funding from the National Science Foundation Office of Polar Programs through grants OPP-0838781  
453 and OPP-1644197 to ARS and RG. The writing of this manuscript was also made possible through the  
454 US-UK Fulbright Commission to ARS for support during his sabbatical at Durham University. This  
455 manuscript benefited by reviews from two anonymous reviewers and special issue editor Glenn Milne.  
456 The PALSEA community is also thanked for inspiring this work.

457

#### 458 **References:**

459 Abram, N.J., Mulvaney, R., Wolff, E.W., Triest, J., Kipfstuhl, S., Trusel, L.D., Vimeux, F., Fleet, L.,  
460 Arrowsmith, C., 2013. Acceleration of snow melt in an Antarctic Peninsula ice core during the  
461 twentieth century. *Nature Geoscience* 6, 404-411.

462 Allen, C.S., Oakes-Fretwell, L., Anderson, J.B., Hodgson, D.A., 2010. A record of Holocene glacial and  
463 oceanographic variability in Neny Fjord, Antarctic Peninsula. *The Holocene* 20, 551-564.

464 Amesbury, M., Roland, T.P., Royles, J., Hodgson, D.A., Convey, P., Griffiths, H., Charman, D.J., 2017.  
465 Widespread biological response to rapid warming on the Antarctic Peninsula. *Current Biology* 27,  
466 1616-1622

467 Aoki, S., 2002. Coherent sea level response to the Antarctic Oscillation. *Geophysical Research Letters* 29,  
468 L015733.

469 Baroni, C., Hall, B.L., 2004. A new Holocene relative sea-level curve for Terra Nova Bay, Victoria Land,  
470 Antarctica. *Journal of Quaternary Science* 19, 377-396.

471 Bassett, S.E., Milne, G.A., Bentley, M.J., Huybrechts, P., 2007. Modelling Antarctic sea-level data to  
472 explore the possibility of a dominant Antarctic contribution to meltwater pulse 1A. *Quaternary*  
473 *Science Reviews* 26, 2113-2127.

474 Bentley, M.J., Hodgson, D.A., Smith, J.A., Cox, N.J., 2005. Relative sea level curves for the South Shetland  
475 Islands and Marguerite Bay, Antarctic Peninsula. *Quaternary Science Reviews* 24, 1203-1216.

476 Birkenmajer, K., 1998. Quaternary geology at Potter Peninsula, King George Island (South Shetland  
477 Islands, West Antarctica). *Bulletin of the Polish Academy of Sciences Earth Sciences* 27, 77-85.

478 Bradley, S.L., Hindmarsh, R.C.A., Whitehouse, P.L., Bentley, M.J., King, M.A., 2015. Low post-glacial  
479 rebound rates in the Weddell Sea due to Late Holocene ice-sheet readvance. *Earth and Planetary*  
480 *Science Letters* 413, 79-89.

481 Bøtter-Jensen, L., McKeever, S. W. S., and Wintle, A. G., 2003, *Optically Stimulated Luminescence*  
482 *Dosimetry*, Amsterdam, Elsevier, 355 p.

483 Butler, E.R.T., 1999. Process environments on modern and raised beaches in McMurdo Sound,  
484 Antarctica. *Marine Geology* 162, 105-120.

485 Cavalieri, D.J., Parkinson, C.L., 2008. Antarctic sea ice variability and trends, 1979-2006. *Journal of*  
486 *Geophysical Research Oceans* 113, C07004.

487 Christ, A.J., Talaia-Murray, M., Elking, N., Domack, E.W., Leventer, A., Lavoie, C., Brachfeld, S., Yoo, K.-C.,  
488 Gilbert, R., Jeong, S.-M., Petrushak, S., Wellner, J.S., LARISSA Group, 2015. Late Holocene glacial  
489 advance and ice shelf growth in Barilari Bay, Graham Land, west Antarctic Peninsula. *Geological*  
490 *Society of America Bulletin* 127, p. 297-315.

491 Clapperton, C.M., Sugden, D.E., 1988. Holocene glacier fluctuations in South America and Antarctica.  
492 *Quaternary Science Reviews* 7, 185-198.

493 Cook, A.J., Fox, A.J., Vaughan, D.G., Ferrigno, J.G., 2005. Retreating glacier fronts on the Antarctic  
494 Peninsula over the past half-century. *Science* 308, 541-544.

495 Curl, J.E., 1980. A glacial history of the South Shetland Islands, Antarctica. *Institute of Polar Studies*  
496 *Report* 63, 1-129.

497 Duller, G.A.T., 2003. Distinguishing quartz and feldspar in single grain luminescence measurements.  
498 *Radiation Measurements* 37, 161-165.

499 Fretwell, P.T., Hodgson, D.A., Watcham, E.P., Bentley, M.J., Roberts, S.J., 2010. Holocene isostatic uplift  
500 of the South Shetland Islands, Antarctic Peninsula, modelled from raised beaches. *Quaternary*  
501 *Science Reviews* 29, 1880-1893.

502 Galbraith, R.F., Roberts, R.G., Laslet, G.M., Yoshida, H., Olley, J.M., 1999. Optical dating of single and  
503 multiple grains of quartz from Jinmium rock shelter, northern Australia: Part I, Experimental  
504 design and statistical models. *Archaeometry* 41, 339-364.

505 Hall, B.L., 2007. Late-Holocene advance of the Collins Ice Cap, King George Island, South Shetland  
506 Islands. *The Holocene* 17, 1253-1258.

507 Hall, B.L., 2010. Holocene relative sea-level changes and ice fluctuations in the South Shetland Islands.  
508 *Global and Planetary Change* 74, 15-26.

509 Hall, B.L., Denton, G.H., 1999. New relative sea-level curves for the southern Scott Coast, Antarctica:  
510 evidence for Holocene deglaciation of the western Ross Sea. *Journal of Quaternary Science* 14,  
511 641-650.

512 Hall, B.L., Koffman, T., Denton, G.H., 2010. Reduced ice extent on the western Antarctic Peninsula at  
513 800-970 cal. yr B.P. *Geology* 38, 635-638.

514 Hamlington, B.D., Leben, R.R., Kim, K.-Y., Nerem, R.S., Atkinson, L.P., Thompson, P.R., 2015. The effect of  
515 the El Nino-Southern Oscillation on U.S. regional and coastal sea level. *Journal of Geophysical*  
516 *Research: Oceans* 120, p. 3970-3986.

517 Hansen, J., Ruedy, R., Glascoe, J., Sato, M., 1999. GISS analysis of surface temperature change. *Journal of*  
518 *Geophysical Research* 104, 30997-31022.

519 Hansom, J.D., Flint, C.P., 1989. Holocene ice fluctuations on Brabant Island, Antarctic Peninsula.  
520 *Antarctic Science* 1: 165-166.

521 Heroy, D.C., Sjunneskog, C., Anderson, J.B., 2008. Holocene climate change in the Bransfield Basin,  
522 Antarctic Peninsula: evidence from sediment and diatom analysis. *Antarctic Science* 20, 69-87.

523 Hjort, C., Ingolfsson, O., Moller, P., Lirio, J.M., 1997. Holocene glacial history and sea-level changes on  
524 James Ross Island, Antarctic Peninsula. *Journal of Quaternary Science* 12, 259-273.

525 Hodgson, D.A., 2011. First synchronous retreat of ice shelves marks a new phase of polar deglaciation.  
526 *Proceedings of the National Academy of Sciences* 108, 18859-18860.

527 Hodgson, D.A., Roberts, S.J., Smith, J.A., Verleyen, E., Sterken, M., Labarque, M., Sabbe, K., Vyverman,  
528 W., Allen, C.S., Leng, M.J., Bryant, C., 2013. Late Quaternary environmental changes in Marguerite  
529 Bay, Antarctic Peninsula, inferred from lake sediments and raised beaches. *Quaternary Science*  
530 *Reviews* 68, 216-236.

531 Ingolfsson, O., Hjort, C., Bjorck, S., Smith, R.J.L., 1992. Late Pleistocene and Holocene glacial history of  
532 James Ross Island, Antarctic Peninsula. *Boreas* 21, 209-222.

533 Ivins, E.R., James, D.P., 2005. Antarctic glacial isostatic adjustment: a new assessment. *Antarctic Science*  
534 17, 541-553.

535 Ivins, E.R., Raymond, C.A., James, T.S., 2000. The influence of 5000 year-old and younger glacial mass  
536 variability on present-day crustal rebound in the Antarctic Peninsula. *Earth, Planets, and Space* 52,  
537 1023-1029.

538 Ivins, E.R., Watkins, M.M., Yuan, D.-N., Dietrich, R., Casassa, G., Rulke, A., 2011. On-land ice loss and  
539 glacial isostatic adjustment at the Drake Passage: 2003-2009. *Journal of Geophysical Research* 116,  
540 B02403.

541 John, B.S., Sugden, D.E., 1971. Raised marine features and phases of glaciation in the South Shetland  
542 Islands. *British Antarctic Survey Bulletin* 24, 45-111.

543 Jourdain, N.C., Mathiot, P., Merino, N., Durand, G., Le Sommer, J., Spence, P., Dutrieux, P., Madec, G.,  
544 2017. Ocean circulation and sea-ice thinning induced by melting ice shelves in the Amundsen Sea.  
545 *Journal of Geophysical Research: Oceans* 122, 2550-2573.

546 Kendall, R.A., Mitrovica, J.X., Milne, G.A., 2005. On post-glacial sea level - II. Numerical formulation and  
547 comparative results on spherically symmetric models. *Geophysical Journal International* 161, 679-  
548 706.

549 Kim, S., Yoo, K.-C., Lee, J.I., Khim, B.-K., Bak, Y.-S., Lee, M.K., Lee, J., Domack, E.W., Christ, A.J., Yoon, H.I.,  
550 2018. Holocene paleoceanography of Bigo Bay, west Antarctic Peninsula: Connections between  
551 surface water productivity and nutrient utilization and its implication for surface-deep water mass  
552 exchange. *Quaternary Science Reviews* 192, 59-70.

553 King, M.A., Bingham, R.J., Moore, P., Whitehouse, P.L., Bentley, M.J., Milne, G.A., 2012. Lower satellite-  
554 gravimetry estimates of Antarctic sea-level contribution. *Nature* 491, 586-589.

555 Landerer, F.W., Jungclaus, J.H., Marotzke, J., 2007. Regional dynamic and steric sea-level change in  
556 response to the IPCC-A1B Scenario. *Journal of Physical Oceanography* 37, 296-312.



557 Leventer, A., Domack, E.W., Ishman, S.E., Brachfeld, S., McClennen, C.E., Manley, P., 1996. Productivity  
558 cycles of 200-300 years in the Antarctic Peninsula region: Understanding linkages among the sun,  
559 atmosphere, oceans, sea ice, and biota. *Geological Society of America Bulletin* 108, 1626-1644.

560 Li, X., Holland, D.M., Gerber, E.P., Yoo, C., 2014. Impacts of the north and tropical Atlantic Ocean on the  
561 Antarctic Peninsula and sea ice. *Nature* 505, 538-542.

562 Lindhorst, S., Schutter, I., 2014. Polar gravel beach-ridge systems: Sedimentary architecture, genesis,  
563 and implications for climate reconstructions (South Shetland Islands/Western Antarctic Peninsula).  
564 *Geomorphology* 221, 187-203.

565 Lorenz, K., Harris, C., 2014. Antarctic Specially Managed Area No. 7: Palmer Station Arthur Harbor.  
566 1:15,000, 2<sup>nd</sup> Edition, Environmental Research and Assessment (ERA).

567 Marshall, G.J., Orr, A., Van Lipzig, N.P.M., King, J.C., 2006. The impact of a changing southern  
568 hemisphere annular mode on Antarctica Peninsula summer temperatures. *Journal of Climate* 19,  
569 5388-5404.

570 McKay, N.P., Overpeck, J.T., Otto-Bliesner, B.L., 2011. The role of ocean thermal expansion in Last  
571 Interglacial sea level rise. *Geophysical Research Letters* 38, L14605.

572 Meredith, M.P., King, J.C., 2005. Rapid climate change in the ocean west of the Antarctic Peninsula  
573 during the second half of the 20<sup>th</sup> Century. *Geophysical Research Letters* 32, L19604.

574 Miles, G.M., Marshall, G.J., McConnell, J.R., Aristarain, A.J., 2008. Recent accumulation variability and  
575 change on the Antarctic Peninsula from the ERA40 reanalysis. *International Journal of Climatology*  
576 28, 1409-1422.

577 Mintenbeck, K., Torres, J.J., 2017. Impact of climate change on the Antarctic silverfish and its  
578 consequences for the Antarctic ecosystem, in: Vacchi, M., Pisano, E., Ghigliotti, L. (Eds.), *The*  
579 *Antarctic Silverfish: a Keystone Species in a Changing Ecosystem*. Springer, pp. 253-286.

580 Minzoni, R.T., Anderson, J.B., Fernandez, R., Wellner, J.S., 2015. Marine record of Holocene climate,  
581 ocean, and cryosphere interactions: Herbert Sound, James Ross Island, Antarctica. *Quaternary*  
582 *Science Reviews* 129, 239-259.

583 Moline, M.A., Karnovsky, N.J., Brown, Z., Divoky, G.J., Frazer, T.K., Jacoby, C.A., Torres, J.J., Fraser, W.R.,  
584 2008. High latitude changes in ice dynamics and their impact on polar marine ecosystems. *Annals*  
585 *of the New York Academy of Sciences* 1134, 267-319.

586 Montes-Hugo, M., Doney, S.C., Ducklow, H.W., Fraser, W., Martinson, D., Stammerjohn, S.E., Schofield,  
587 O., 2009. Recent changes in phytoplankton communities associated with rapid regional climate  
588 change along the western Antarctic Peninsula. *Science* 323, 1470-1473.

589 Mulvaney, R., Abram, N.J., Hindmarsh, R.C.A., Arrowsmith, C., Fleet, L., Triest, J., Sime, L.C., Alemany, O.,  
590 Foord, S., 2012. Recent Antarctic Peninsula warming relative to Holocene climate and ice-shelf  
591 history. *Nature advance online publication*.

592 Murray, A.S., Wintle, A.G., 2000. Luminescence dating of quartz using an improved single-aliquot  
593 regenerative-dose protocol. *Radiation Measurements* 32, 57-73.

594 Murray, A.S., Wintle, A.G., 2003. The single aliquot regenerative dose protocol: potential for  
595 improvements in reliability. *Radiation Measurements* 37, 377-381.

596 Nakada, M., Lambeck, K., 1988. The melting history of the Late Pleistocene Antarctic Ice-Sheet. *Nature*  
597 333, 36-40.

598 Nichols, R.L., 1960. Geomorphology of Marguerite Bay Area, Palmer Peninsula, Antarctica. *Geological*  
599 *Society of America Bulletin* 71, 1421-1450.

600 Nield, G.A., Barletta, V.R., Bordoni, A., King, M.A., Whitehouse, P.L., Clarke, P.J., Domack, E., Scambos,  
601 T.A., Berthier, E., 2014. Rapid bedrock uplift in the Antarctic Peninsula explained by viscoelastic  
602 response to recent ice unloading. *Earth and Planetary Science Letters* 397, 32-41.

603 Nield, G.A., Whitehouse, P.L., King, M.A., Clarke, P.J., Bentley, M.J., 2012. Increased ice loading in the  
604 Antarctic Peninsula since the 1850s and its effect on glacial isostatic adjustment. *Geophysical*  
605 *Research Letters* 39, L17504.

606 Orsi, A.J., Cornuelle, B.D., Severinghaus, J.P., 2012. Little Ice Age cold interval in West Antarctica:  
607 Evidence from borehole temperature at the West Antarctic Ice Sheet (WAIS) Divide. *Geophysical*  
608 *Research Letters* 39, L09710.

609 Pallas, R., James, T.S., Sabat, F., Vilaplana, J.M., Grant, D.R., 1997. Holocene uplift in the South Shetland  
610 Islands; evaluation of tectonics and glacio-isostasy, in: Ricci, C.A. (Ed.), *The Antarctic region;*  
611 *geological evolution and processes; Proceedings of the VII international symposium on Antarctic*  
612 *earth sciences.* Terra Antarctica Publication, Italy.

613 Peltier, W.R., 2004. Global glacial isostasy and the surface of the ice-age Earth: the ICE-5G (VM2) model  
614 and GRACE. *Annual Review of Earth and Planetary Sciences* 32, 111-149.

615 Porat, N., Duller, G. A. T., Roberts, H. M., and Wintle, A. G., 2009, A simplified SAR protocol for TTOSL:  
616 *Radiation Measurements*, v. 44, p. 538-542.

617 Reilly, B.T., Natter, C.J.Jr., Brachfeld, S.A., 2016. Holocene glacial activity in Barilari Bay, west Antarctic  
618 Peninsula, tracked by magnetic mineral assemblages: Linking ice, ocean, and atmosphere.  
619 *Geochemistry, Geophysics, Geosystems* 17, 4553-4565.

620 Rhodes, E. J., 2011, Optically stimulated luminescence dating of sediments over the past 200,000 years:  
621 *Annual Review of Earth and Planetary Sciences*, v. 39, p. 461-488. Rignot, E., Bamber, J.L., van den  
622 Broeke, M.R., Davis, C., Li, Y., van der Berg, W.J., van Meijgaard, E., 2008. Recent Antarctic ice  
623 mass loss from radar interferometry and regional climate modelling. *Nature Geoscience* 1, 106-  
624 110.

625 Rink W., Thompson J. (Ed.) Earth Sciences Series. Encyclopedia of Scientific Dating Methods:  
626 SpringerReference (www.springerreference.com). Springer-Verlag Berlin Heidelberg, 2013. DOI:  
627 10.1007/SpringerReference\_359042

628 Roberts, S.J., Hodgson, D.A., Sterken, M., Whitehouse, P.L., Verleyen, E., Vyverman, W., Sabbe, K., Balbo,  
629 A., Bentley, M.J., Moreton, S.G., 2011. Geological constraints on glacio-isostatic adjustment  
630 models of relative sea-level change during deglaciation of Prince Gustav Channel, Antarctic  
631 Peninsula. *Quaternary Science Reviews* 30, 3603-3617.

632 Rott, H., Skvarca, P., Nagler, T., 1996. Rapid collapse of Northern Larsen Ice Shelf, Antarctica. *Science*  
633 271, 788-792.

634 Shepherd, A., Ivins, E.R., A, G., Barletta, V.R., Bentley, M.J., Bettadpur, S., Briggs, K.H., Bromwich, D.H.,  
635 Forsberg, R., Galin, N., Horwath, M., Jacobs, S., Joughin, I., King, M.A., Lenaerts, J.T.M., Li, J.,  
636 Ligtenberg, S.R.M., Luckman, A., Luthcke, S.B., McMillan, M., Meister, R., Milne, G., Mouginit, J.,  
637 Muir, A., Nicolas, J.P., Paden, J., Scambos, T.A., Scheuchl, B., Schrama, E.J.O., Smith, B., Sundal,  
638 A.V., van Angelen, J.H., van de Berg, W.J., Van den Broeke, M.R., Vaughan, D.G., Velicogna, I.,  
639 Wahr, J., Whitehouse, P.L., Wingham, D.J., Yi, D., Young, D., Zwally, H.J., 2012. A reconciled  
640 estimate of ice-mass balance. *Science* 338, 1182-1189.

641 Shevenell, A.E., Ingalls, A.E., Domack, E.W., Kelly, C., 2011. Holocene Southern Ocean surface  
642 temperature variability west of the Antarctic Peninsula. *Nature* 470, 250-254.

643 Shevenell, A.E., Kennett, J.P., 2002. Antarctic Holocene climate change: a benthic foraminiferal stable  
644 isotope record from Palmer Deep. *Nature* 470, 250-254.

645 Sime, L.C., Marshall, G.J., Mulvaney, R., Thomas, E.R., 2009. Interpreting temperature information from  
646 ice cores along the Antarctic Peninsula: ERA40 analysis. *Geophysical Research Letters* 36, L18801.

647 Simkins, L.M., DeWitt, R., Simms, A.R., 2013a. Methods to reduce sample carrier contamination for  
648 luminescence measurements. *Ancient TL* 31, 19-28.

649 Simkins, L.M., DeWitt, R., Simms, A.R., Briggs, S., Shapiro, R.S., 2016. Investigation of optically stimulated  
650 luminescence behavior of quartz from crystalline rock surfaces: A look forward. *Quaternary*  
651 *Geochronology* 36, 161-173.

652 Simkins, L.M., Simms, A.R., DeWitt, R., 2013b. Relative sea-level history of Marguerite Bay, Antarctic  
653 Peninsula derived from optically stimulated luminescence-dated beach cobbles. *Quaternary*  
654 *Science Reviews* 77, 141-155.

655 Simkins, L.M., Simms, A.R., DeWitt, R., 2015. Assessing the link between coastal morphology, wave  
656 energy and sea ice throughout the Holocene from Antarctic raised beaches. *Journal of Quaternary*  
657 *Science* 30, 335-348.

658 Simms, A.R., DeWitt, R., Kouremenos, P., Drewry, A.M., 2011. A new approach to reconstructing sea  
659 levels in Antarctica using optically stimulated luminescence of cobble surfaces. *Quaternary*  
660 *Geochronology* 6, 50-60.

661 Simms, A.R., Ivins, E.R., DeWitt, R., Kouremenos, P., Simkins, L.M., 2012. Timing of the most recent  
662 Neoglacial advance and retreat in the South Shetland Islands, Antarctic Peninsula: Insights from  
663 raised beaches and Holocene uplift rates. *Quaternary Science Reviews* 47, 41-55.

664 Smith, R.I.L., 1982. Plant succession and re-exposed moss banks on a deglaciated headland in Arthur  
665 Harbour, Anvers Island. *British Antarctic Survey Bulletin* 51, 193-199.

666 Taylor, J.R., 1997. *An Introduction to Error Analysis*. 2<sup>nd</sup> Edition. University Science Books, Sausalito,  
667 California. 327 p.

668 Thomas, I.D., King, M.A., Bentley, M.J., Whitehouse, P.L., Penna, N.T., Williams, S.D.P., Riva, R.E.M.,  
669 Lavallee, D.A., Clarke, P.J., King, E.C., Hindmarsh, R.C.A., Koivula, H., 2011. Widespread low rates of  
670 Antarctic glacial isostatic adjustment revealed by GPS observations. *Geophysical Research Letters*  
671 38, L22302.

672 Thompson, L.G., Peel, D.A., Mosley-Thompson, E., Mulvaney, R., Dai, J., Lin, P.N., Davis, M.E., Raymond,  
673 C.F., 1994. Climate since AD 1510 on Dyer Plateau, Antarctic Peninsula: evidence for recent  
674 climate change. *Annals of Glaciology* 20, 420-426.

675 Van der Wal, W., Whitehouse, P.L., Schrama, E.J.O., 2015. Effect of GIA models with 3D mantle viscosity  
676 on GRACE mass balance estimates for Antarctica. *Earth and Planetary Science Letters* 414, 134-  
677 143.

678 Vaughan, D.G., Doake, C.S.M., 1996. Recent atmospheric warming and retreat of ice shelves on the  
679 Antarctic Peninsula. *Nature* 379, 328-331.

680 Vaughan, D.G., Marshall, G.J., Connolley, W.M., Parkinson, C., Mulvaney, R., Hodgson, D.A., King, J.C.,  
681 Pudsey, C.J., Turner, J., 2003. Recent rapid regional climate warming on the Antarctic Peninsula.  
682 *Climate Change* 60, 243-274.

683 Wallinga, J., 2002. Optically stimulated luminescence dating of fluvial deposits: a review. *Boreas* 31, 303-  
684 322.

685 Watcham, E.P., Bentley, M.J., Hodgson, D.A., Roberts, S.J., Fretwell, P.T., Lloyd, J.M., Larter, R.D.,  
686 Whitehouse, P.L., Leng, M.J., Monien, P., Moreton, S.G., 2011. A new Holocene sea level curve for  
687 the South Shetland Islands, Antarctica. *Quaternary Science Reviews* 30, 3152-3170.

688 Whitehouse, P.L., Bentley, M.J., Le Brocq, A.M., 2012a. A deglacial model for Antarctica: geological  
689 constraints and glaciological modelling as a basis for a new model of Antarctic glacial isostatic  
690 adjustment. *Quaternary Science Reviews* 32, 1-24.

691 Whitehouse, P.L., Bentley, M.J., Milne, G.A., King, M.A., Thomas, I.D., 2012b. A new glacial isostatic  
692 adjustment model for Antarctica: calibrated and tested using observations of relative sea-level  
693 change and present-day uplift rates. *Geophysical Journal International* 190, 1464-1482.

694 Wintle, A.G., Murray, A.S., 2006. A review of quartz optically stimulated luminescence characteristics  
695 and their relevance in single-aliquot regeneration dating protocols. *Radiation Measurements* 41,  
696 369-391.

697 Wolstencroft, M., King, M.A., Whitehouse, P.L., Bentley, M.J., Nield, G.A., King, E.C., McMillan, M.,  
698 Shepherd, A., Barletta, V., Bordoni, A., Riva, R.E.M., Didova, O., Gunter, B.C., 2015. Uplift rates  
699 from a new high-density GPS network in Palmer Land indicate significant late Holocene ice loss in  
700 the southwestern Weddell Sea. *Geophysical Journal International* 203, 737-754.

701 Yoon, H.I., Yoo, K.-C., Bak, Y.-S., Lim, H.S., Kim, Y., Lee, J.I., 2010. Late Holocene cyclic glaciomarine  
702 sedimentation in a subpolar fjord of the South Shetland Islands, Antarctica, and its  
703 paleoceanographic significance: Sedimentological, geochemical, and paleontological evidence.  
704 *Geological Society of America Bulletin* 122, 1298-1307.

705 Zhao, C., King, M.A., Watson, C.S., Barletta, V.R., Bordoni, A., Dell, M., Whitehouse, P.L., 2017. Rapid ice  
706 unloading in the Fleming Glacier region, southern Antarctic Peninsula, and its effect on bedrock  
707 uplift rates. *Earth and Planetary Science Letters* 473, 2017.

708 Zwart, D., Bird, M., Stone, J., Lambeck, K., 1998. Holocene sea-level change and ice-sheet history in the  
709 Vestfold Hills, East Antarctica. *Earth and Planetary Science Letters* 155, 131-145.

710

711 **Figure Captions:**

712

713 **Figure 1.** Map of the northern Antarctic Peninsula illustrating the locations of places mentioned in the  
714 text.

715 **Figure 2.** A) Aerial photograph of Torgersen Island and Palmer Station Region (from GoogleEarth). B)  
716 Inset map showing the location of (A) with respect to locations shown in Figure 1 as well as Biscoe Point  
717 and Litchfield Island. C) Photograph of the raised beaches at Torgersen Island.

718 **Figure 3.** Model predictions of the rate of sea-surface height change (SSH) from 1.54 ka to 0.79 ka (A)  
719 and 0.79 ka to the present (B) using the ice model of Whitehouse et al. (2012b). The difference in the  
720 rate of SSH height change predicted using the ice model of Whitehouse et al. (2012) and a modified ice  
721 model with 10% less ice at 1.0 ka and 10% more ice at 0.5 ka at 1.54 ka to 0.79 ka (C) and 0.79 ka to  
722 present (D). All predictions are for Palmer Station, Antarctica.

723 **Figure 4.** Changes in uplift rates through time from GPS observations at Palmer Station (Nield et al.,  
724 2014 and Thomas et al., 2011) and Holocene relative sea-level indicators at Beak Island (Roberts et al.,  
725 2011; this study) and Torgersen Island (this study). See Figure 1 for locations.

726 **Figure 5.** Glacial isostatic adjustment model results of relative sea-level changes (RSL, black lines) at  
727 Torgersen Island, deconvolved into the solid earth (DEF, red lines) and sea-surface height components  
728 (blue lines) with the original ice model of Whitehouse et al. (2012a)(A, B) and a modified ice model (C)  
729 with a 10% decrease in the ice thickness at 1.0 ka and a 10% increase in the ice at 0.5 ka (see text for  
730 details). See Figure 1 for location of Torgersen Island.

731

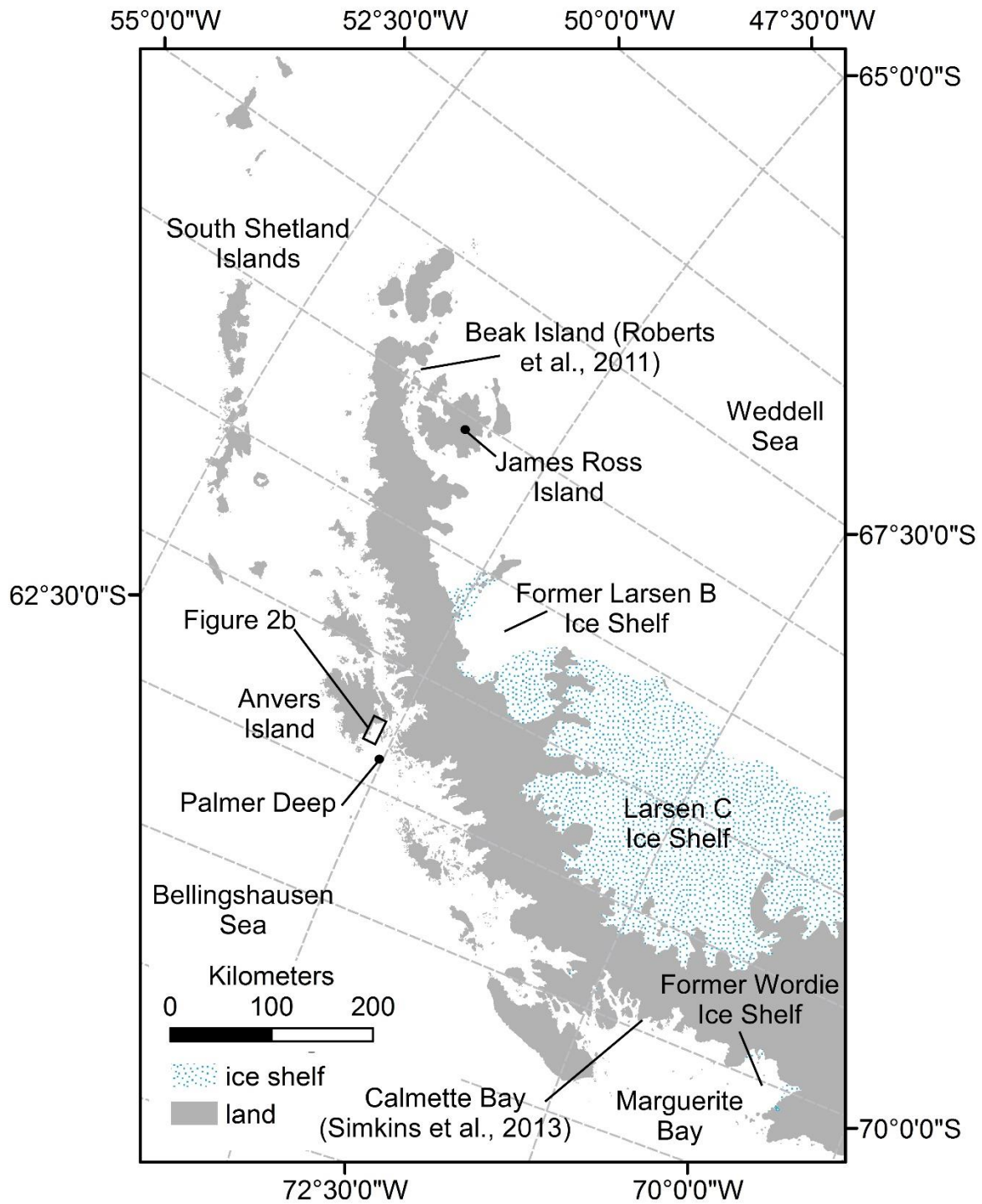
732 **Table 1.** OSL ages from the southern margin of Anvers Island, western Antarctic Peninsula

733 **Table 2.** Uplift rate calculations for Torgersen Island, Antarctic Peninsula

734

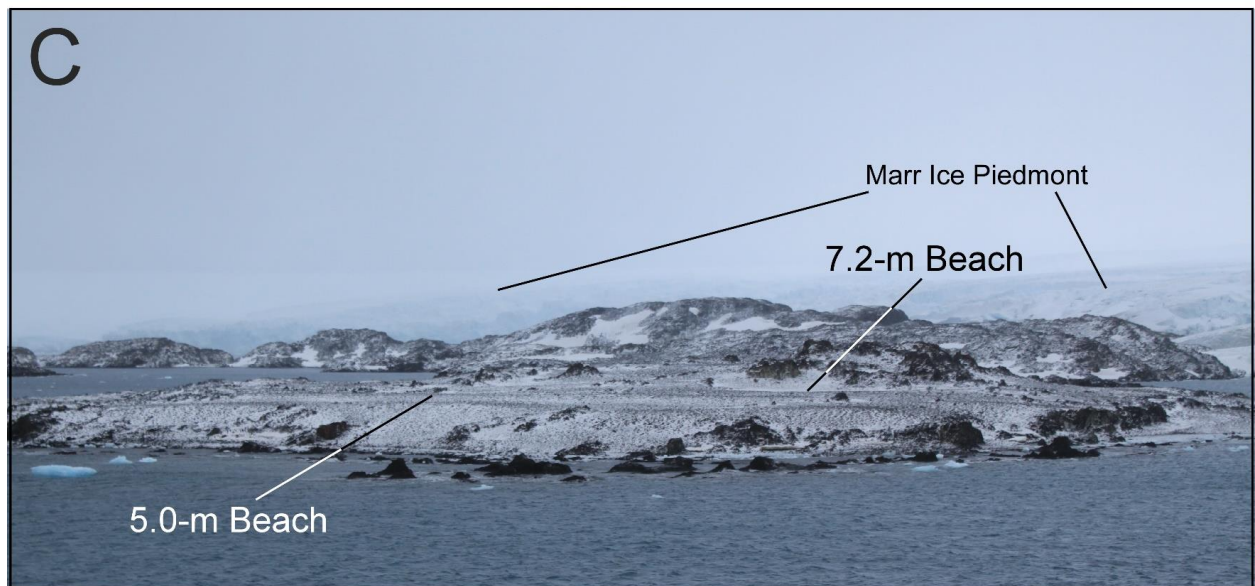
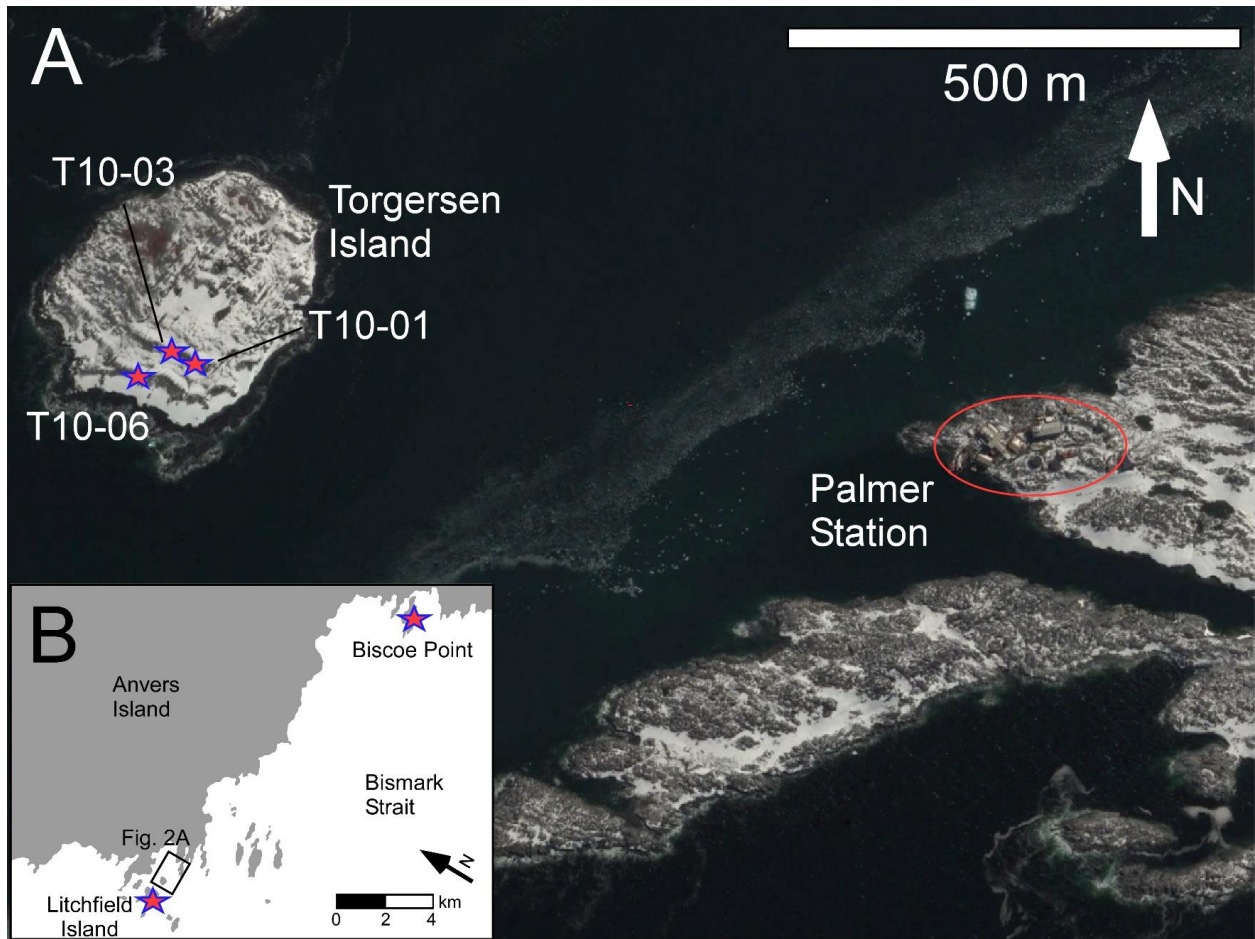
735





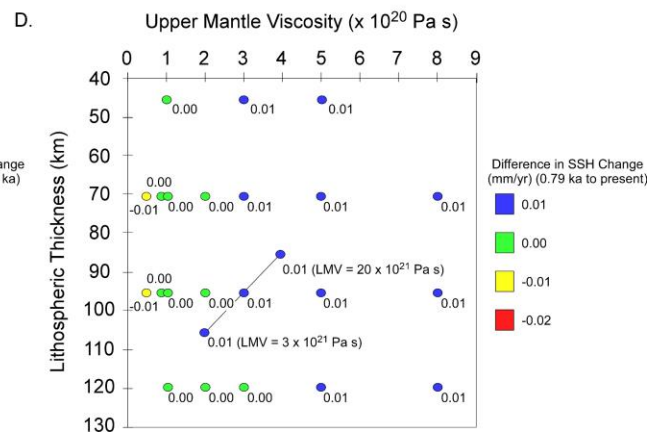
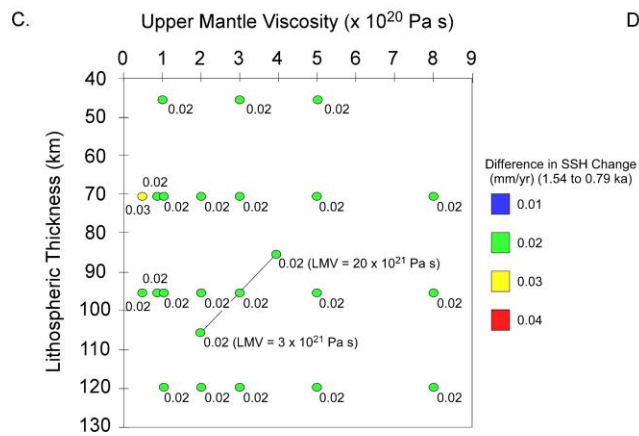
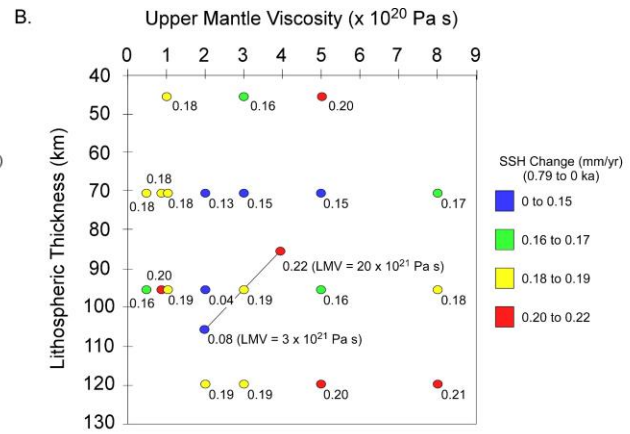
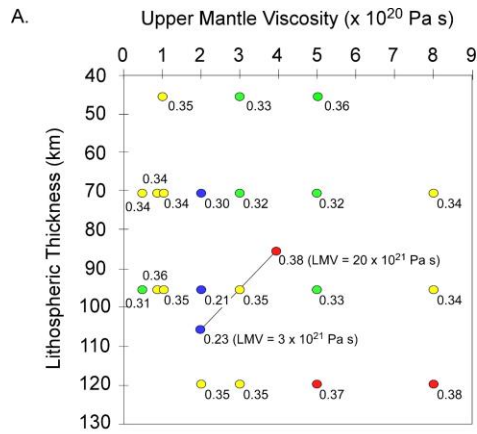
736

737 Figure 1.



738

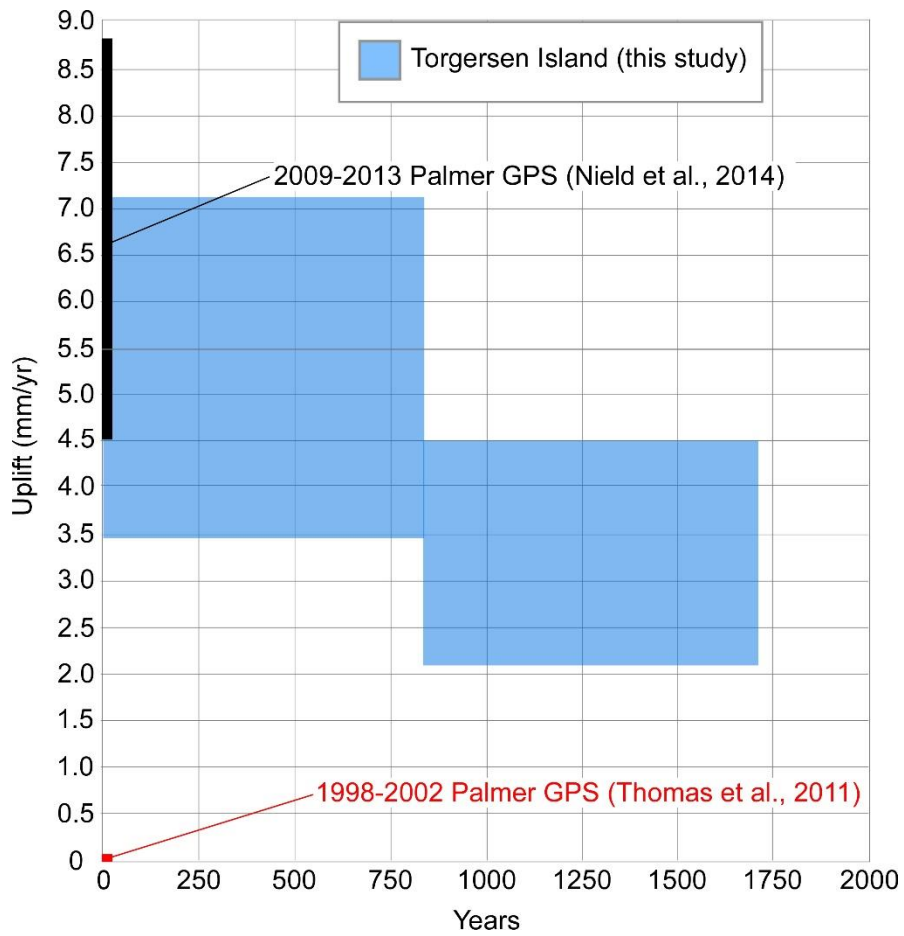
739 Figure 2.



740

741 Figure 3.

742

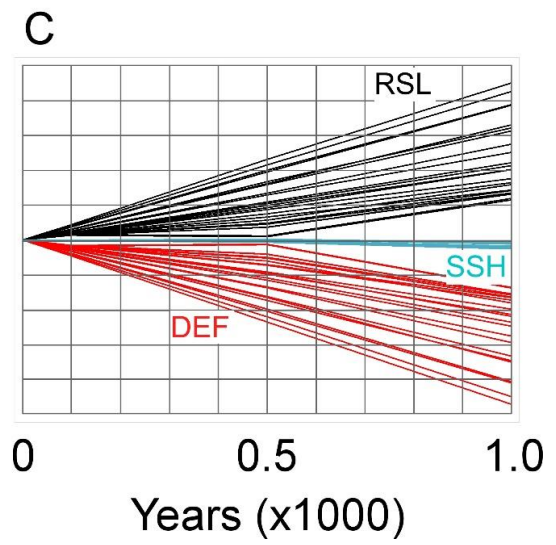
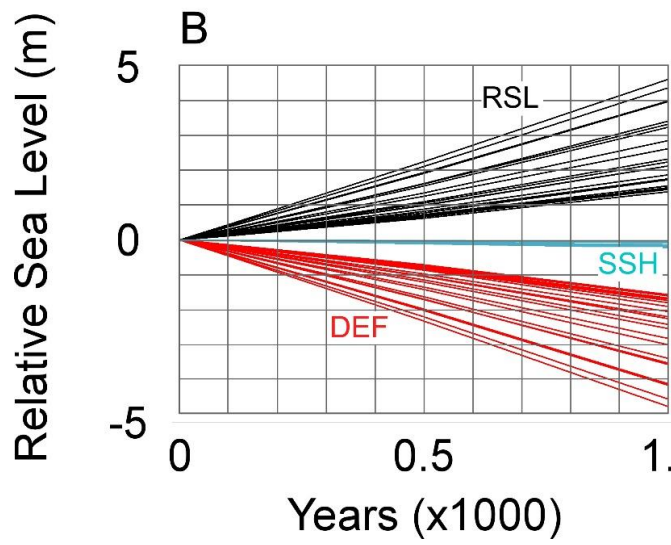
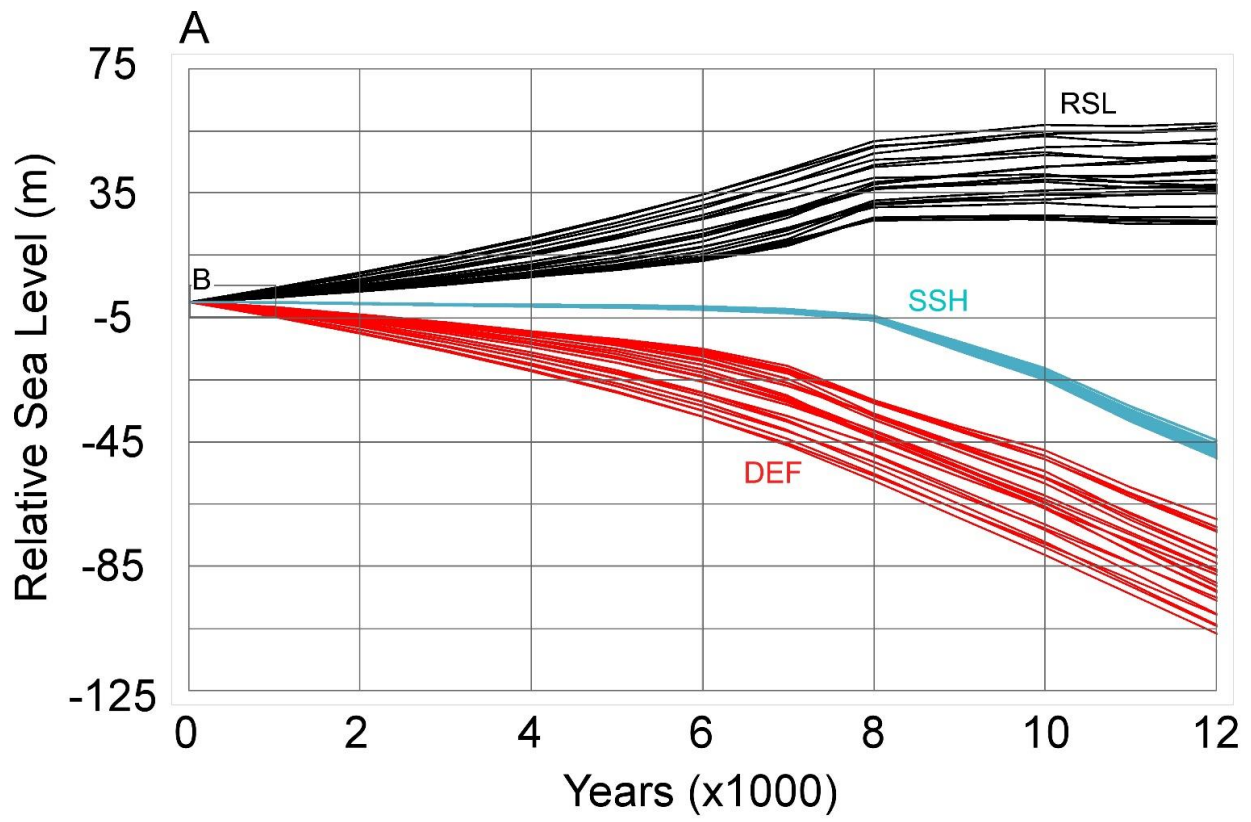


743

744 Figure 4.

745





746

747 Figure 5.

748

749

**Table 1.** OSL ages from Anvers Island, western Antarctic Peninsula

Sample	Location (Lat., Long.) <sup>*</sup>	Elev. (m asl.)	Aliquots <sup>†</sup>	D <sub>e</sub> (Gy)	DR (Gy ky <sup>-1</sup> )	Age (a) <sup>‡</sup>	Source
Torgersen Island							
T10-06	64.7732, 64.0765	5.0	14	1.18 ± 0.08	1.48 ± 0.14	790 ± 180	Simkins <i>et al.</i> (2015)
T10-03	64.7732, 64.0757	7.2	15	3.42 ± 0.14	2.32 ± 0.13	1480 ± 200	Simkins <i>et al.</i> (2015)
T10-01	64.7731, 64.0758	7.2	8	2.43 ± 0.21	1.11 ± 0.14	2180 ± 680	Simkins <i>et al.</i> (2015)
Litchfield Island							
LI10-08	64.7720, 64.0889	0.5	6	0	Not measured	Modern	This study
Biscoe Point							
BP10-01	64.81667, 63.81667	2	6	0	Not measured	Modern	This study
BP10-02	64.81667, 63.81667	2	6	0	Not measured	Modern	This study
BP10-05	64.81667, 63.81667	2	6	0	Not measured	Modern	This study

Elev. (elevation); D<sub>e</sub> (equivalent dose); DR (dose rate); ky (thousand years); a (years)

<sup>\*</sup> In decimal degrees.

<sup>†</sup> Aliquots presented pass all standard SAR procedure tests, with the exception of modern samples that only were measured in initial dose tests.

<sup>‡</sup> Ages are rounded to the nearest ten years. Ages date beach formation and errors are reported as 2σ.

750

751 Table 1.

752

**Table 2.** Uplift rate calculations for Torgersen Island, Antarctic Peninsula

Time Period (cal BP)	RSL Rate (mm/yr)	Error (mm/yr)	SH-Correctio (mm/yr)	SH-Correction Erro (mm/yr)	Uplift Rate (mm/yr)	Error (mm/yr)
0-790	5.1	1.8	0.2	0.1	5.3	1.8
790-1540	3	1.2	0.3	0.1	3.3	1.2
<b>Difference (mm/yr)</b>	2.1	2.2			2.0	2.2

SSH (sea surface height)

\*Error calculated as to incorporate the age uncertainty of the marine-lacustrine sedimentary contact

753

754 Table 2.